Superelasticity in bcc nanowires by a reversible twinning mechanism

Suzhi Li,[1] Xiangdong Ding,[1,2,*,†] Junkai Deng,[1,3] Turab Lookman,[2,*,‡] Ju Li,[1,4] Xiaobing Ren,[1,3] Jun Sun,[1] and Avadh Saxena[2]

[1]*State Key Laboratory for Mechanical Behavior of Materials, Xi'an Jiaotong University, Xi'an 710049, China*

[2]*Theoretical Division, Los Alamos National Laboratory, Los Alamos, New Mexico 87545, USA*

[3]*Ferroic Physics Group, National Institute for Materials Science, Tsukuba, 305-0047 Ibaraki, Japan*

[4]*Department of Materials Science and Engineering, University of Pennsylvania, Philadelphia, Pennsylvania 19104, USA*

(Received 10 May 2010; revised manuscript received 27 October 2010; published 29 November 2010)

Superelasticity (SE) in bulk materials is known to originate from the structure-changing martensitic transition which provides a volumetric thermodynamic driving force for shape recovery. On the other hand, structure-invariant deformation processes, such as twinning and dislocation slip, which result in plastic deformation, cannot provide the driving force for shape recovery. We use molecular-dynamics simulations to show that some bcc metal nanowires exhibit SE by a "reversible" twinning mechanism, in contrast to the above conventional point of view. We show that this reversible twinning is driven by the surface energy change between the twinned and detwinned state. In view of similar recent findings in fcc nanowires, we suggest that SE is a general phenomenon in cubic nanowires and that the driving force for the shape recovery arises from minimizing the surface energy. Furthermore, we find that SE in bcc nanowires is unique in several respects: first, the $\langle 111\rangle/\{112\}$ stacking fault generated by partial dislocation is always preferred over $\langle 111\rangle/\{110\}$ and $\langle 111\rangle/\{123\}$ full dislocation slip. The occurrence of $\langle 111\rangle/\{112\}$ twin or full dislocation slip in bcc nanowires depends on the competition between the emission of subsequent partial dislocations in adjacent {112} planes and the emission of partial dislocations in the same plane. Second, compared to their fcc counterparts, bcc nanowires have a higher energy barrier for the nucleation of twins, but a lower energy barrier for twin migration. This results in certain unique characteristics of SE in bcc nanowires, such as low energy dissipation and low strain hardening. Third, certain refractory bcc nanowires, such as W and Mo, can show SE at very high temperatures, which are higher than almost all of the reported high-temperature shape memory alloys. Our work provides a deeper understanding of superelasticity in nanowires and refractory bcc nanowires are potential candidates for applications in nanoelectromechanical systems operating over a wide temperature range.

DOI: 10.1103/PhysRevB.82.205435 PACS number(s): 62.25.−g, 62.23.Hj, 61.72.Mm, 68.35.Md

I. INTRODUCTION

Superelasticity (SE) is a characteristic property of shape-memory alloys (SMAs) which have been widely studied over several decades due to their applications as sensors, actuators, and microeletromechanical devices.[1–3] In general, superelasticity is based on the phase stability of thermoelastic martensite: a stress-induced martensitic transformation during loading and the reverse-martensitic transformation during unloading.[4] In contrast, deformation of bulk crystals is often controlled by the motion of dislocations or deformation twins, processes that result in plastic deformation and thus cannot usually recover after unloading.

However, nanosized materials possess the feature that the surface energy (negligible for bulk materials) becomes important and this can lead to novel properties not expected in bulk materials.[5–9] Recently, molecular-dynamics (MD) simulations have shown that a class of fcc metals[10–15] in the form of nanowires can exhibit SE via a twinning mechanism. For example, in single-crystalline Cu, Ag, and Ni metallic nanowires, the initially created $\langle 100\rangle/\{100\}$ nanowires can spontaneously reorient to a defect-free $\langle 110\rangle/\{111\}$ structure above a critical temperature.[10,12,15] Interestingly, under uniaxial tension, the reoriented $\langle 110\rangle/\{111\}$ wire can exhibit SE by transforming to the initial $\langle 100\rangle/\{100\}$ configuration via movement of twin boundaries.[11–15] This mechanism for SE has not been previously considered and is quite different from that associated with bulk SMAs.[1] It has been well accepted that the large surface energy difference between the twinned and detwinned configurations as well as the movement of twins are the two major factors that dominate this unique behavior.[10–12,14] The minimization of surface energy for a nanowire provides the thermodynamic driving force whereas the reversible twin boundary motion provides a crystallographic pathway for the complementary reorientation. However, this phenomenon has mainly focused on fcc nanowires to date and it is unclear whether this effect is common to nanowires possessing other crystal structures, in particular nonclose packed lattices.

The purpose of this work is to use the MD simulation approach to explore superelasticity in bcc nanowires via a similar twinning mechanism as in fcc nanowires. Our results show that some bcc nanowires also deform superelastically via a mechanism that involves minimization of surface energy and twin boundary motion. Our work emphasizes that superelasticity is a general phenomenon in cubic metal nanowires where both the large surface energy difference and reversible twinning deformation play key roles. Moreover, we find that in contrast to fcc nanowires, the SE of bcc nanowires is unique in several respects: (i) the $\langle 111\rangle/\{112\}$ stacking fault generated by the $\frac{a}{6}\langle 111\rangle$ partial dislocation is always preferred to the $\langle 111\rangle/\{110\}$ and $\langle 111\rangle/\{123\}$ full dislocation slip. The occurrence of the $\langle 111\rangle/\{112\}$ twin or full dislocation slip in bcc nanowires depends on the competition

between the emission of subsequent $\frac{a}{6}\langle 111\rangle$ partial dislocations in adjacent {112} planes and the emission of $\frac{a}{3}\langle 111\rangle$ partial dislocations in the same {112} plane. (ii) bcc nanowires face a higher energy barrier for nucleating twins but a lower barrier for twin migration, compared to their fcc counterparts. This results in unique characteristics related to SE in bcc nanowires, such as low energy dissipation and low strain hardening. (iii) Certain refractory bcc nanowires, such as W and Mo, show SE at very high temperatures, which are higher than almost all of the reported high-temperature SMAs.[16,17] Hence, our work has the potential to impact applications of materials showing superelasticity in nanoelectromechanical systems operating over a wide temperature range.

The outline of the paper is as follows. In Sec. II, we present the simulation method, whereas Sec. III focuses on the simulation results. In Sec. IV, we analyze the driving force for superelasticity in bcc nanowires, and consider the competition between twinning and full-dislocation slip in these nanowires. Superelasticity in fcc and bcc nanowires is then compared and we conclude with Sec. V.

II. SIMULATION METHOD

In our MD simulations we focus on nanowires of iron,[18] vanadium,[19] tungsten,[20] and molybdenum[20] using embedded-atom method (EAM) (Ref. 21) potentials which reproduce relatively good thermomechanical properties of the above bcc element metals, such as the cohesive energy, elastic constants, and the low-index surface energies (especially the surface energy difference between the low-index surfaces, which play a crucial role in the present calculations), etc.[18–20] However, one should not expect that such semiempirical potentials can reproduce all the properties of the metals. The initial bcc nanowires were first created along the $x-[100], y-[011], z-[0\bar{1}1]$ directions at 0 K. The wires have dimensions of $50a\times 5\sqrt{2}a\times 5\sqrt{2}a$, where a is the lattice constant at 0 K (0.31472 nm, 0.31652 nm, 0.28553 nm, and 0.30299 nm for Mo, W, Fe, and V, respectively). We then relaxed the initial nanowires at 300 K for almost 1000 picoseconds to obtain an equilibrium state by using the Nosé-Hoover thermostat.[22,23] The relaxed wires were then loaded in the x direction with atoms at the ends fixed to play the role of loading grips. The tensile strain was applied by a ramp velocity profile to give the minimum strain at one fixed end and maximum at the other. Unloading was performed in a similar manner by applying a reverse ramp velocity that was terminated when the stress was reduced to zero. The strain rate during loading/unloading was 10^7 s^{-1} and the MD calculations were carried out using the LAMMPS code[24] with the atomic configurations displayed by ATOMEYE.[25]

III. RESULTS

A. Superelasticity in Mo, W, and Fe nanowires

The mechanical behavior of a Mo nanowire was first tested under unixial tension. Figure 1(a) shows the stress-strain curve of the Mo nanowire upon loading and unloading at 300 K. We see that in the loading stage, after a short elastic deformation to the yield point of 16.2 GPa, the stress drops dramatically to a relatively low value. Further loading causes an extensive plateau stage with stress remaining at approximately 2.2 GPa. Upon unloading, the plastic strain can almost fully recover along the same pathway as the loading process to exhibit classic superelastic behavior with a total recoverable strain exceeding 40%.

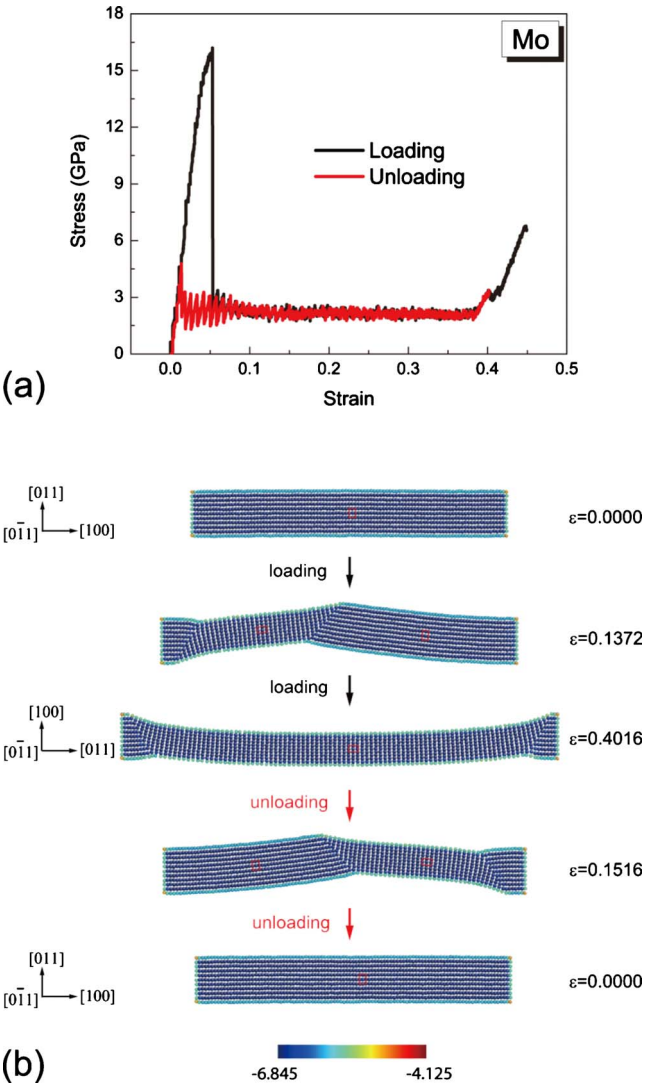

FIG. 1. (Color online) Illustration of superelasticity at 300 K in a Mo nanowire with dimensions of 15.74 nm×2.23 nm ×2.23 nm. (a) Stress-strain curve of the Mo nanowire during the loading and unloading process. The recoverable strain can exceed 40%. (b) The corresponding atomic configurations due to mechanical deformation (only two adjacent lattice planes are shown for each snapshot). Upon loading, the [100]-axis configuration transforms to the [011]-axis configuration with the aid of twinning. The lattice unit cell rotates by 90° to produce the crystal reorientation. Subsequently, upon unloading the [011]-axis nanowire reverts back through reversible twin boundary motion. Atoms are colored according to the values of their potential energy in the unit of eV.

By observing the corresponding atomic configurations during loading/unloading, we find that twinning/detwinning is the underlying mechanism responsible for the reversible strain. As shown in Fig. 1(b), upon tensile loading the newly

formed $\langle 111\rangle/\{112\}$ single twin divides the whole nanowire into three domains. As strain increases, the twin boundaries further propagate toward the ends and the whole wire transforms from the initial orientation $(x-[100], y-[011], z-[0\bar{1}1])$ to the new configuration $(x-[011], y-[100], z-[0\bar{1}1])$ with a 90° rotation of the unit cell in the xy plane. For convenience, we hereafter refer to the initial and reoriented configurations of the wire as [100] and [011], respectively. When the system is unloaded, detwinning follows the reverse path to allow the wire to recover its original shape. The presently observed SE due to twinning is similar to that shown in fcc nanowires.[10–14]

We further investigated the mechanical behavior of W and Fe nanowires under uniaxial tension. Figures 2(a) and 2(b) show the stress-strain curves of W and Fe wires at 300 K, respectively. From Figs. 2(a) and 2(b), we clearly see that the SE also exists in W and Fe nanowires. Atomic configurations (not shown here) corroborate that the SE of W and Fe nanowires is also mediated by a twinning/detwinning mechanism, as for Mo nanowires. One interesting observation is that the stress-strain curves for Mo, W, and Fe [Figs. 1(a), 2(a), and 2(b)] during unloading follow almost their loading curves. This suggests that the SE of Mo, W, and Fe wires is characteristic of low-energy dissipation, which is quite different from the SE in fcc nanowires.[11,12,14]

B. Irreversible deformation in V nanowires

Unlike Mo, W, and Fe wires, the vanadium (V) nanowire failed to exhibit any SE under unixial tension. As shown in Fig. 2(c), V nanowires first deform elastically during loading. Upon yielding, necking occurs and this quickly leads to thinning and eventual rupture of the wire. While twinning/detwinning is responsible for the superelasticity in Mo, W, and Fe wires, $\langle 111\rangle/\{112\}$ dislocation slip is primarily responsible for the thinning and eventual rupture process in V nanowires [shown later in Fig. 5(d)]. The slip mechanism, involving full dislocations, causes the tensile deformation to be permanent and irreversible upon unloading. Consequently, no superelasticity is possible for V nanowires.

C. Effect of strain rate on the superelasticity in Mo, W, and Fe nanowires

Our MD simulations are performed with the strain rate of 10^7 s^{-1}. Although it is already very slow for MD simulations, it is an extremely high strain rate compared to reality. Previously, work related to fracture have reported twinning as a mechanism at high strain rates in iron but with slower rates a dislocation mechanism takes over.[26,27] To verify whether the observed superelasticity mediated by the twinning mechanism in our simulations is dependent on the strain rate, we further checked the deformation behavior of Mo, W, and Fe nanowires under quasistatic conditions by using an annealing MD method. To perform this calculation, we first applied a prescribed strain (0.014%) to the relaxed [100]-oriented nanowires through the fixed atomic layers at the ends at 0 K and then minimized the energy of the nanowire using the conjugate-gradient (CG) method. By repeating the above process, we completed the tensile deformation of the wires. Unloading follows a similar path by applying a negative strain increment.

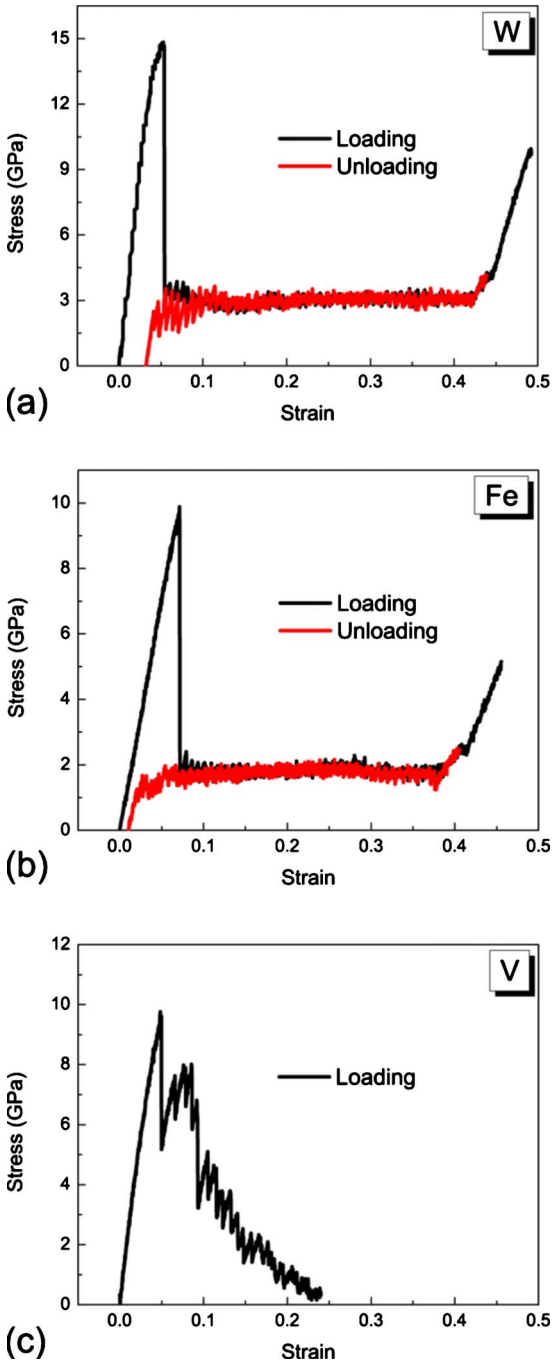

FIG. 2. (Color online) Stress-strain curves for W, Fe, and V nanowires at 300 K. Figures 2(a) and 2(b) show the superelasticity with the aid of twin deformation in a W and Fe nanowire, respectively. Figure 2(c) shows the failure of superelasticity in the V nanowire due to the activation of full-dislocation slip.

Figures 3(a)–3(c) show the calculated stress-strain curves for Mo, W, and Fe nanowires which have dimensions of $50a \times 5\sqrt{2}a \times 5\sqrt{2}a$, where a is lattice constant at 0 K. It is clear that, even under quasistatic loading/unloading at 0 K, W, Mo, and Fe nanowires can still exhibit almost perfect or

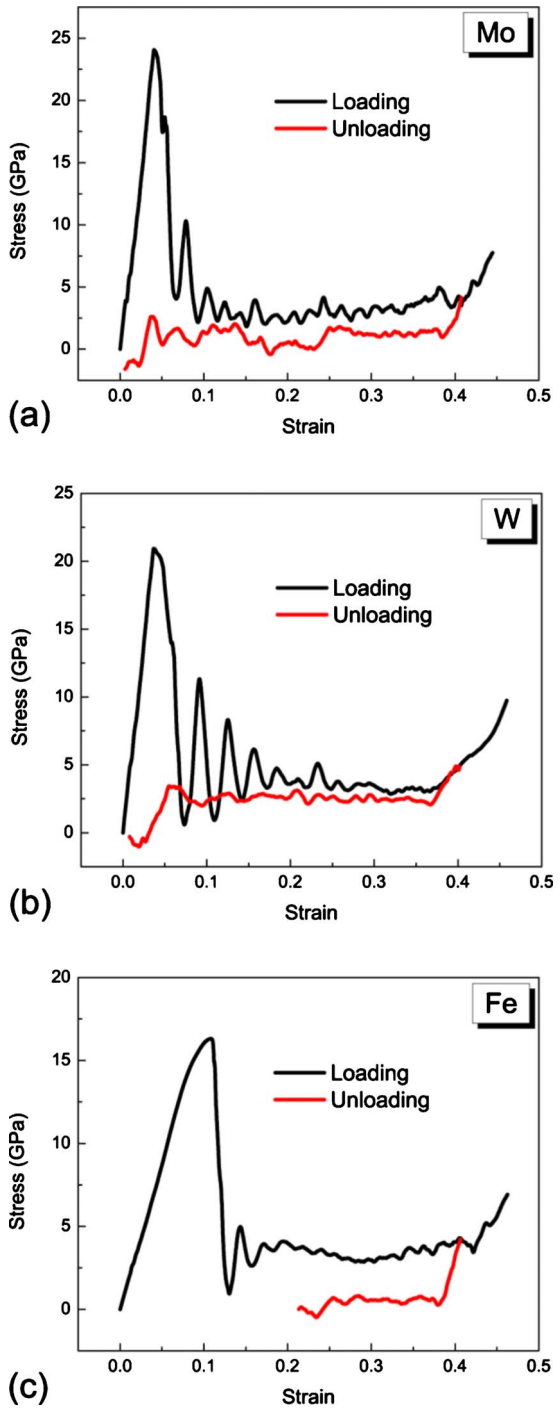

FIG. 3. (Color online) Stress-strain curves of Mo, W, and Fe nanowires with dimensions of $50a \times 5\sqrt{2}a \times 5\sqrt{2}a$ using annealing MD methods. (a) and (b) show that Mo and W are able to exhibit good superelasticity with more than 40% recoverable strain, and (c) shows Fe nanowire can exhibit partial superelasticity.

partial SE. Further, atomic configurations show that the SE of W, Mo, and Fe nanowires are still mediated by a twinning/detwinning mechanism, similar to the cases of loading/unloading at 300 K with high strain rate [as shown in Fig. 1(b)]. This indicates that the reversible twinning behavior we found in W, Mo, and Fe nanowires is independent of the strain rate. In addition, we noticed that the recoverable strain

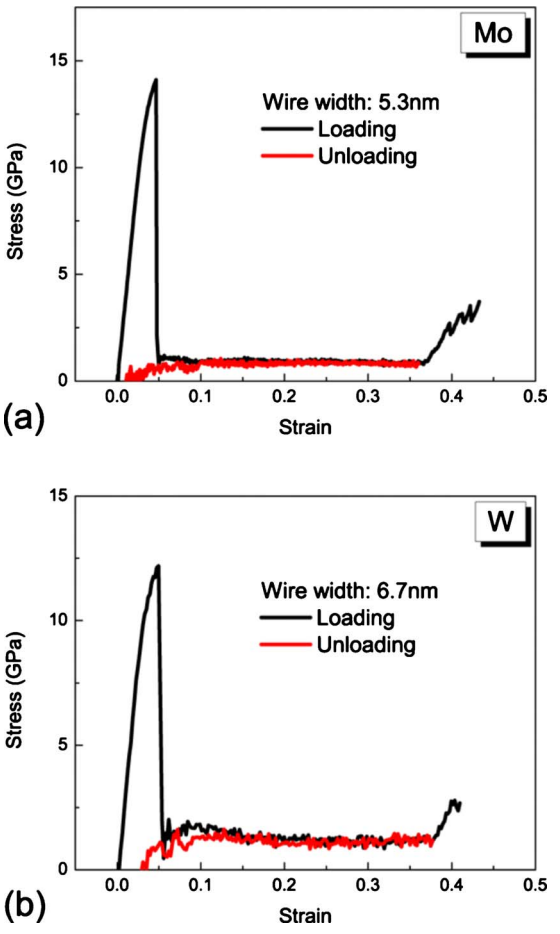

FIG. 4. (Color online) Stress-strain curves for a (a) 5.3-nm-width Mo and (b) 6.7-nm-width W nanowire at 300 K. Both show excellent superelasticity.

in W, Mo, and Fe nanowires is different at 0 K, indicating that the mobility of twins in these three metals (Mo, W, and Fe) at nanoscale is diffident and we will discuss it later (Secs. IV B and IV C).

D. Size effect on the superelasticity in Mo and W nanowires

The present calculations already show SE in W, Mo, and Fe nanowires with a small cross sectional size ($5\sqrt{2}a$, about 2.2 nm, 2.2 nm, and 2.0 nm, respectively). It is interesting to determine whether such an effect can be found in larger sizes, closer to realistic cases. For this purpose, we took W and Mo nanowires as examples, and studied the effect of the cross-sectional size on the superelasticity at 300 K by keeping the aspect ratio as $5\sqrt{2}$.

Figure 4(a) shows that the stress-strain curve for a 5.3-nm-width Mo nanowire upon loading and unloading. We observed that the Mo nanowire still exhibits almost perfect superelasticity. In addition, Fig. 4(b) shows that a W nanowire can also exhibit superelasticity even when the cross-sectional size reached 6.7 nm. As the current ability to synthesize nanowires with tunable diameters has reached 1.6 nm (Ref. 28) or even down to approximately 0.8 nm,[29] e.g., gold nanowires formed by electron-beam irradiation in an ultrahigh

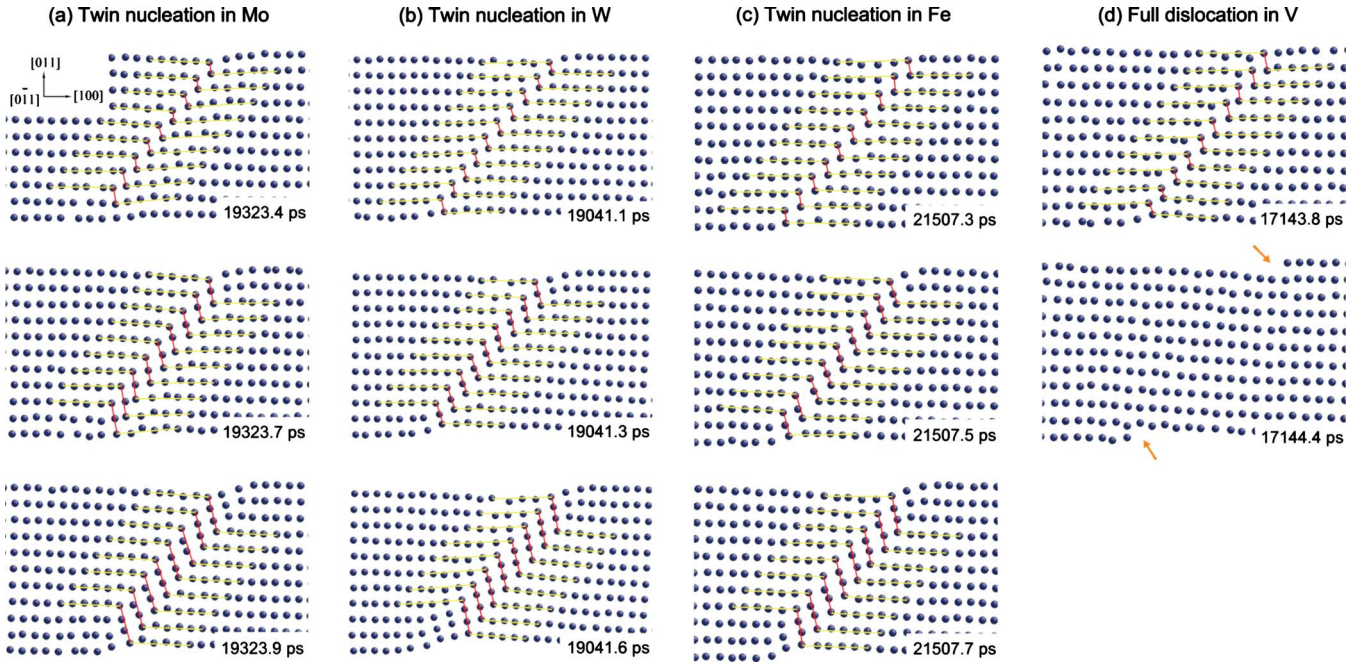

FIG. 5. (Color online) The atomic images of the incipient plasticity upon loading in Mo, W, Fe, and V nanowires. Figure 5(a)–5(c) show the snapshots of twin nucleation in Mo, W, and Fe, respectively (only two adjacent lattice planes are shown for each snapshot). Using Mo as a typical example, a stacking fault forms at first from the perfect nanowires. The embryo subsequently forms in a layer-by-layer manner with respect to the stacking fault. Yellow lines denote the stacking layers along the original [100] axis of the nanowire. Red lines refer to the newly formed microtwin. Figure 5(d) shows the full-dislocation slip in the V nanowire, leaving a step at the surface indicated by the arrows.

vacuum electron microscope have a thickness of 0.8–3 nm and a length of 5–10 nm.[29] The present size (e.g., 5.3 nm or 6.7 nm) of the nanowire already reaches dimensions that can be perfectly fabricated in experiments.[28,29]

E. Atomic processes for twin formation and full dislocation slip

From the above discussions, we note that superelasticity in Mo, W, and Fe nanowires is mediated by reversible movement of twin boundaries, whereas the plastic deformation of V nanowires is related to the irreversible slip of full dislocations. However, we would like to understand the corresponding atomic processes underlying the formation and growth of twins and full dislocation slip. We therefore consider the nature of the atomic configurations at the initial plastic deformation of the above nanowires.

As shown in Figs. 5(a)–5(c), we see that the formation and growth of twins in Mo, W, and Fe nanowires is quite similar: the nanowire first forms a one-layer of stacking faults (SF) from the perfect crystal through a $\frac{a}{6}[111]$ partial dislocation in the $\{\bar{2}11\}$ plane, followed by a second stacking fault with $\frac{a}{6}[111]$ partial dislocation in the adjacent $\{\bar{2}11\}$ plane. These layer-by-layer stacking processes through sliding of $\frac{a}{6}[111]$ partial dislocations in adjacent $\{\bar{2}11\}$ planes finally cause the formation and growth of twins in Mo, W, and Fe nanowires. As for the V nanowire [shown in Fig. 5(d)], we see that the first SF with a $\frac{a}{6}[111]$ partial dislocation is also easy to form along the $\{\bar{2}11\}$ plane. However, the second $\frac{a}{6}[111]$ partial fails to be activated in the adjacent $\{\bar{2}11\}$ planes. Rather, another $\frac{a}{3}[111]$ partial dislocation is emitted along the same $\{\bar{2}11\}$ layer and results in the formation of a full dislocation $\frac{a}{2}[111]$ in the specific $\{\bar{2}11\}$ plane.

To further understand the growth process for $\langle 111\rangle/\{112\}$-type twins in bcc nanowires, we focus on the formation of SFs during tension at 300 K. The results show that the growth of $\langle 111\rangle/\{112\}$ twins in bcc nanowires involves a consecutive movement of $\frac{a}{6}[111]$ partial dislocations in adjacent $\{\bar{2}11\}$ planes. As illustrated in Fig. 6, initially a partial dislocation is nucleated at one side of the free surface of the Mo nanowire [Fig. 6(a)] and then slides along the [111] direction in the $\{\bar{2}11\}$ planes gradually [Figs. 6(b) and 6(c)]. It finally moves out of the crystal at the opposite side leading to the formation of a one-layer SF. Subsequently, another partial dislocation is nucleated in a similar way [Fig. 6(d)] to generate yet another partial dislocation in the successive $\{\bar{2}11\}$ plane. Through this repeatable process, the growth of twinning is accomplished. The progress of twin motion is quite similar to that in a fcc nanowire, which is related to the sliding of $\frac{a}{6}\langle 112\rangle$ partial dislocations in adjacent {111} planes.[14]

IV. DISCUSSION

A. Driving force for superelasticity of bcc nanowires

It is well known that twinning in bulk materials is one of the deformation modes which induces permanent plastic strain upon unloading.[30,31] The present superelasticity in Mo, W, and Fe nanowires implies that detwinning mediated by

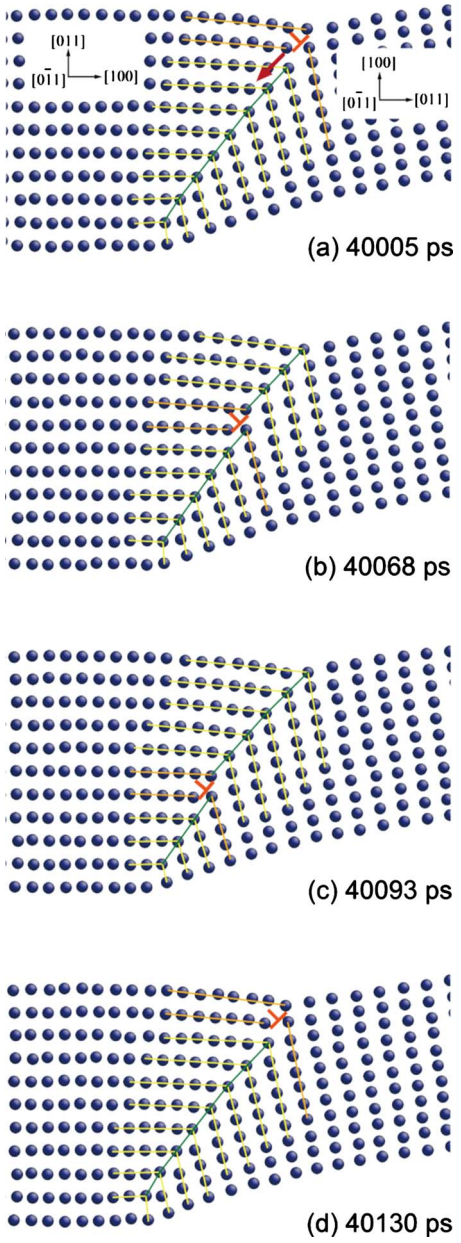

FIG. 6. (Color online) Twinning propagation process in a Mo nanowire (only two adjacent lattice planes are shown for each snapshot). A $\frac{a}{6}[111]$ partial dislocation nucleates on one side of the surface, propagates and annihilates in the $(\bar{2}11)$ planes. The consecutive partial dislocation at free surface then follows a similar process. Red arrow indicates the slip direction of the partial dislocation. Green line denotes the twin boundary. Yellow line denotes the symmetric atomic stacking beside the twin boundary. Orange line indicates the mismatch of atomic layers caused by the movement of partial dislocations.

reverse twin boundary motion can occur spontaneously during unloading. It also indicates that there should be some intrinsic force to drive the reversible twin boundary motion.

The driving force for spontaneous reversible twin boundary motion in Mo, W, and Fe nanowires is mainly due to the reduction of surface energy of the nanowires, similar to that in fcc nanowires.[11,12,32] Taking Mo as an example, Fig. 7

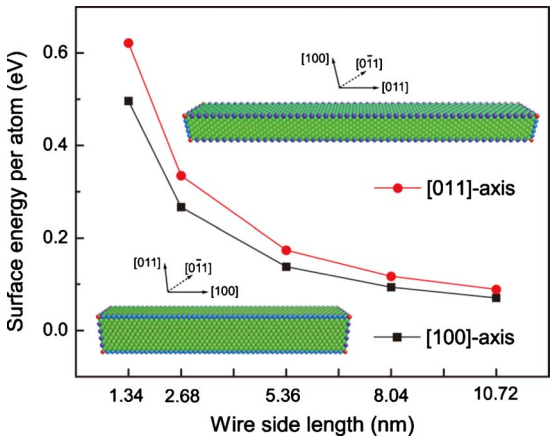

FIG. 7. (Color online) The size-dependent surface energy difference per atom between the [100]-axis and [011]-axis configurations in Mo nanowires at 300 K. With decreasing size, the energy difference increases.

shows the averaged surface energy per atom of the perfect [100]-axis and [011]-axis Mo nanowires as a function of the cross-sectional size of nanowire at 300 K. From this figure, we clearly see that, compared to the original [100]-axis configuration, the reoriented [011]-axis configuration has a higher surface energy per atom, providing the driving force to transform back to the [100] configuration upon unloading. In addition, the surface energy difference between the two configurations increases nonlinearly with decreasing cross section of the nanowire. This indicates that superelasticity becomes easier to induce in small cross-section nanowires and the shape recovery ability becomes weaker or even vanishes for larger cross-section nanowires.

B. Generalized stacking fault energy (GSFE) of twinning and full dislocation slip in bcc nanowires

Our simulation results have shown that Mo, W, and Fe nanowires can exhibit SE through reversible twinning, whereas V nanowires do not show such behavior due to the emission of full dislocation sliding. Thus, bcc nanowires that exhibit SE are strongly influenced by the competition between twinning and full dislocation slip. Therefore, it is natural to ask why some bcc single-crystalline nanowires (e.g., Mo, W, and Fe) can undergo twinning and not the full-dislocation slip, and others (e.g., V) do not show this behavior.

In fcc nanowires the problem can be understood in terms of the GSFE.[33–36] However, because of periodic boundary conditions in directions parallel to the shear planes, the influence of surface energy change during the shearing process is ignored. As a result, the GSFE derived so far only reflects the characteristics of fcc bulk materials but cannot represent the true properties of nanoscale systems. Here we extend this method to bcc nanowires by including the effects of surface energy changes during the shearing process to obtain the GSFE for twinning and full-dislocation slip. We first establish a model for twinning and full-dislocation slip in bcc nanowires, and then calculate the GSFE of twinning and full-

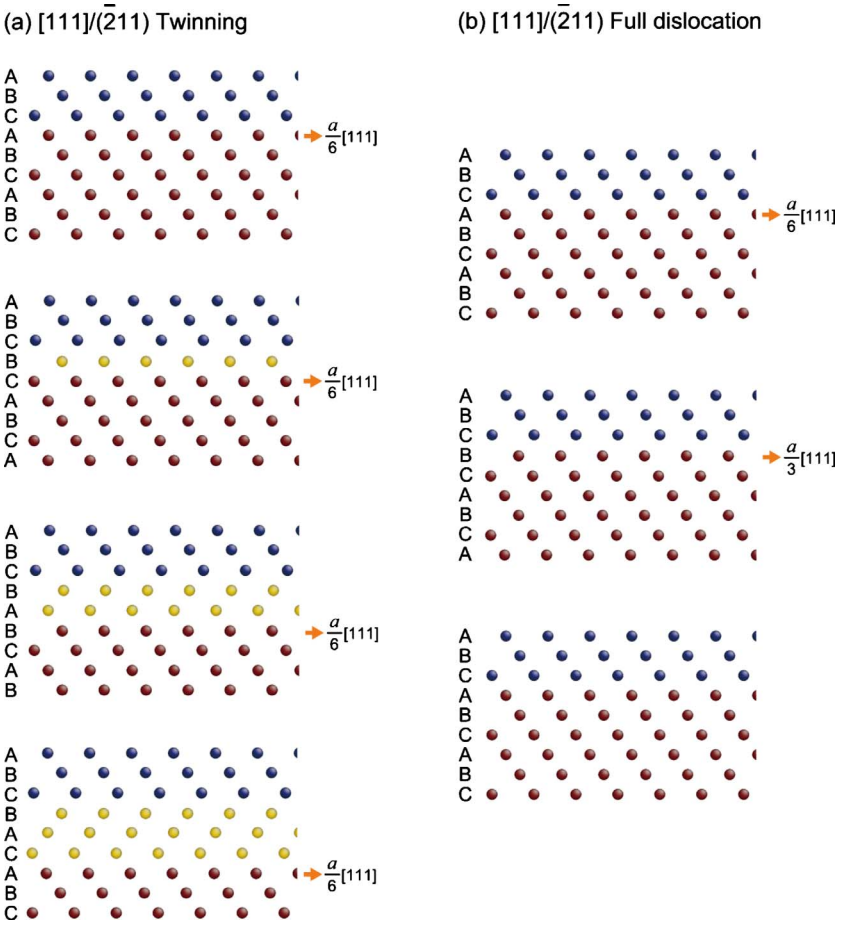

FIG. 8. (Color online) A schematic illustration of full-dislocation slip and deformation twinning in the $\langle 111\rangle/\{112\}$ system of bcc nanowires. Atomic configuration of a bcc perfect crystal with a periodic stacking sequence as $\cdots$ABCABCABC$\cdots$ viewed along $[0\bar{1}1]$ directions. Two nearest atoms in the horizontal direction have a Burgers vector of $\frac{a}{2}[111]$. (a) Twin deformation. For each step, the atoms in the red part shear to $\frac{a}{6}[111]$, which produces the same displacement as in the adjacent $(\bar{2}11)$ planes leading to the stacking sequence change. (b) Process of full dislocation slip in two steps, involving the continued emission of $\frac{a}{6}[111]$ and $\frac{a}{3}[111]$ partials in the same $(\bar{2}11)$ plane. After sliding, the stacking sequence has no change.

dislocation slip in Mo, W, Fe, and V nanowires.

To begin this analysis, we first confirm the deformation process involving the two competing modes (full-dislocation slip and twinning) in bcc nanowires. Based on the simulation results in Fig. 5, we propose a model to explain the $\langle 111\rangle/\{112\}$-type twinning mechanism of bcc nanowires, a process related to the piling of $\frac{a}{6}\langle 111\rangle$ partial dislocations. Here we just use a specific $[111]/(\bar{2}11)$ system to illustrate these processes. The stacking sequence of $(\bar{2}11)$ planes in the bcc system can be regarded as $\cdots$ABCABCABC$\cdots$ layers. A full dislocation with Burgers vector $\frac{a}{2}[111]$ can dissociate into two partials

$$\frac{a}{2}[111] \rightarrow \frac{a}{6}[111] + \frac{a}{3}[111].$$

The nucleation and growth of twins can be ascribed to the emission of $\frac{a}{6}[111]$ partial dislocations on a series of adjacent $(\bar{2}11)$ planes, as shown in Fig. 8(a) schematically. First, a $\frac{a}{6}[111]$ partial slides in the $(\bar{2}11)$ plane to produce a displacement of $\frac{\sqrt{3}a}{6}$ along the [111] direction to form a stacking fault, leading to the alternating stacking sequence $\cdots$ABCBCABCA$\cdots$. Then another $\frac{a}{6}[111]$ partial emits in the neighboring $(\bar{2}11)$ planes to change the sequence to $\cdots$ABCBABCAB$\cdots$. The subsequent partials similarly follow to further allow for twin nucleation and growth. In the present work, we calculated the GSFE curve for twinning up to three layers.

Next, we determine the progress of full dislocation sliding. It is known that there are three main dislocation slip systems in bcc metals, i.e., $\langle 111\rangle/\{112\}$ [specifically, a $\frac{a}{2}[111]$ full dislocation slip along the $(\bar{2}11)$ plane], $\langle 111\rangle/\{110\}$ and $\langle 111\rangle/\{123\}$.[37,38] Since all the sliding processes follow similarly, here we only illustrate with the $\langle 111\rangle/\{112\}$ slip. As shown in Fig. 8(b), the emission of a $\frac{a}{2}[111]$ full dislocation can be regarded as leading $\frac{a}{6}[111]$ and trailing $\frac{a}{3}[111]$ partial slip in the same $(\bar{2}11)$ plane. After emitting the full dislocation, the atomic stacking sequence does not change; it still remains the perfect $\cdots$ABCABCABC$\cdots$ sequence.

On the basis of the above models of twinning and full-dislocation slip, we can calculate the GSFE for bcc nanowires. We first create the bcc nanowires with $50a \times 5\sqrt{2}a \times 5\sqrt{2}a$ (a is the lattice constant at 0 K), the same dimensions as the initial model of the present MD simulations. Shear is then applied to the nanowires to reproduce the $\frac{a}{2}[111]$ full dislocation slip along {112}, {110}, and {123} planes and the $\langle 111\rangle/\{112\}$ twin according to the dynamical process shown in Figs. 8(a) and 8(b). During this process, atoms in the two directions that are perpendicular to the shear direction are relaxed by means of CG algorithm. As a result, we obtain the changes in potential energy with the shear displacement r. Taking the $\langle 111\rangle/\{112\}$ full dislocation slip and twin of Mo nanowire as an example (shown in Fig.

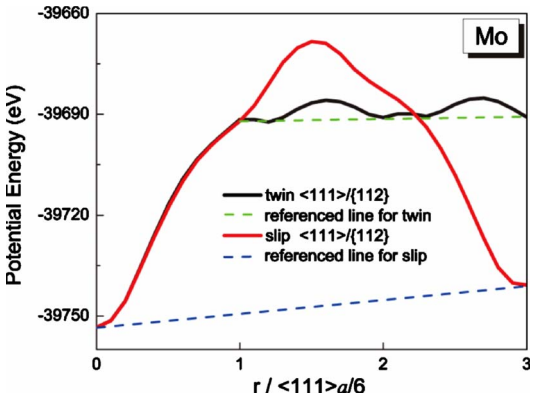

FIG. 9. (Color online) Potential energy change with respect to the number of $\frac{a}{6}[111]$ partials between twining (black solid line) and full-dislocation slip (red solid line) for $\langle 111\rangle/\{112\}$ systems of Mo nanowires with dimensions of $50a\times 5\sqrt{2}a\times 5\sqrt{2}a$, where a is the lattice constant at 0 K. The dashed lines are the reference for eliminating the tilting of the curve. The blue dashed line is the reference line to emit the first partial as well as for full-dislocation slip. The green dashed line is the reference line for the emission of the second and the third partials for twinning.

9), we note that the calculated potential energy-shear displacement curves are no longer periodic as that of bulk materials,[33,39–41] instead they are tilted toward a high-energy state due to the newly created ledge in the side surface of the wire. To obtain the energy change due to the formation of a stacking fault, one needs to eliminate the energy induced by the newly created ledge in the surface. Here, we used a similar method as in Ref. 42, to eliminate such effect by subtracting the inclined lines (blue dashed line in Fig. 9) from the original tilted curves. For the $\langle 111\rangle/\{112\}$ twin (black solid line in Fig. 9), the energy change due to the first $\frac{a}{6}[111]$ partial should be the same as the $\langle 111\rangle/\{112\}$ full dislocation (red solid line in Fig. 9) slip because they follow the same dynamical process. For the second and third $\frac{a}{6}[111]$ partial dislocations, an inclined line that connects the starting and finishing points (green dashed line in Fig. 9) is also used as a reference to remove the effect of newly created ledges. The obtained curves after the above treatment were then normalized by dividing the energy by their original sliding areas in the nanowire. Finally we plot the GSFE curves with an integer number of $\frac{a}{6}[111]$ partial distance.

Figures 10(a)–10(d) show the calculated GSFE curves with the integer number of $\frac{a}{6}[111]$ partial distance for Mo, W, Fe, and V nanowires. The curves in different crystals show similar morphology. Using the Mo nanowire as an example, the single solid line and three dashed lines in Fig. 10(a) represent twinning deformation and three full-dislocation slip systems, respectively. We see that the GSFE curve of the $\langle 111\rangle/\{112\}$ twin can be divided into two stages: First, there is a high energy barrier (γ^{sf}) for emitting the first $\frac{a}{6}[111]$ partial to form a SF from the initial perfect crystal. The shape of the GSFE curve for the emission of subsequent $\frac{a}{6}[111]$ partials is similar to a periodic wave with peaks and valleys. We define the difference between a peak and a valley of the wave as $\Delta\gamma^{\mathrm{twin}}$. Because $\Delta\gamma^{\mathrm{twin}}$ is the energy barrier of emission of subsequent $\frac{a}{6}[111]$ partials on the adjacent $(\bar{2}11)$ planes in the presence of a pre-exiting SF, it is related to the energy barrier for the subsequent formation of twin layers. From Fig. 10(a), we also see that the GSFE curves among different dislocation-slip systems are similar, there is a peak in the GSFE curve indicating the maximum energy barrier for the emission of a full dislocation from the perfect crystal, and we define the peak value as the unstable stacking fault energy γ^{us}. Besides, the difference in γ^{us} and γ^{sf} indicates the energy barrier to form a full dislocation in the presence of a pre-exiting SF, and we define it as $\Delta\gamma^{\mathrm{slip}}$. In addition, we note that the GSFE curve for full dislocation slip in the $\langle 111\rangle/\{112\}$ system is the same as that for $\langle 111\rangle/\{112\}$ twinning before the emission of the first $\frac{a}{6}[111]$ partial dislocation.

C. Competition between twinning and full-dislocation slip in bcc nanowires

Based on the above GSFE curves, we are now ready to investigate the competition between twinning and full-dislocation slip in bcc nanowires and understand the difference in deformation in Mo, W, Fe, and V nanowires. Our analyses show that a SF generated by the $\frac{a}{6}[111]/(\bar{2}11)$ partial dislocation is always preferred over the $\langle 111\rangle/\{110\}$ and $\langle 111\rangle/\{123\}$ full-dislocation slip systems in bcc nanowires. However, whether $\langle 111\rangle/\{112\}$ twinning or $\langle 111\rangle/\{112\}$ full-dislocation occurs in bcc nanowires depends on the competition between subsequent emission of $\frac{a}{6}[111]$ partials in the neighboring $(\bar{2}11)$ planes and the emission of $\frac{a}{3}[111]$ in the same $(\bar{2}11)$ plane. If the former is selected, then $\langle 111\rangle/\{112\}$ twin is preferred; otherwise $\langle 111\rangle/\{112\}$ full dislocation slip will be stimulated in the bcc nanowires.

We first discuss why Mo, W, and Fe bcc single-crystalline nanowires can undergo SE mediated by twinning deformation whereas V nanowires can only endure permanent plastic deformation through full-dislocation slip. According to our previous analysis, the necessary condition to form a twin from the perfect nanowire is the formation of stacking fault emitted by one $\frac{a}{6}[111]/(\bar{2}11)$ partial dislocation. This leads to a tendency to form a twin by further emission of $\frac{a}{6}[111]$ partial dislocations in adjacent $(\bar{2}11)$ planes. On the other hand, if one of the three full-dislocation slip systems is activated from the perfect crystal, the bcc perfect crystal should overcome the unstable stacking fault (γ^{us}). Obviously, the slip system with $\min\{\gamma^{\mathrm{us}}\}$, which is a minimum of γ^{us} among the γ^{us110}, γ^{us112}, γ^{us123} in $\langle 111\rangle/\{110\}$, $\langle 111\rangle/\{112\}$, and $\langle 111\rangle/\{123\}$ slip systems, is more likely to be activated. Since γ^{sf} and $\min\{\gamma^{\mathrm{us}}\}$ characterize the difficulty of forming twinning partial dislocation and full-dislocation slip, we then use the $\gamma^{\mathrm{sf}}/\min\{\gamma^{\mathrm{us}}\}$ ratio to describe the competition between these two deformation modes. Clearly, if $\gamma^{\mathrm{sf}}/\min\{\gamma^{\mathrm{us}}\}>1$, full-dislocation slip is preferred; if $\gamma^{\mathrm{sf}}/\min\{\gamma^{\mathrm{us}}\}<1$, a stacking fault induced by a $\frac{a}{6}[111]/(\bar{2}11)$ partial dislocation is easier at the initial stage of deformation.

Table I lists the calculated γ^{us} for different slip systems, γ^{sf}, $\Delta\gamma^{\mathrm{twin}}$, $\Delta\gamma^{\mathrm{slip}}$, and $\gamma^{\mathrm{sf}}/\min\{\gamma^{\mathrm{us}}\}$ for W, Mo, Fe, and V nanowires. To make a comparison, we also calculated the above parameters in bulk, which are based on the traditional

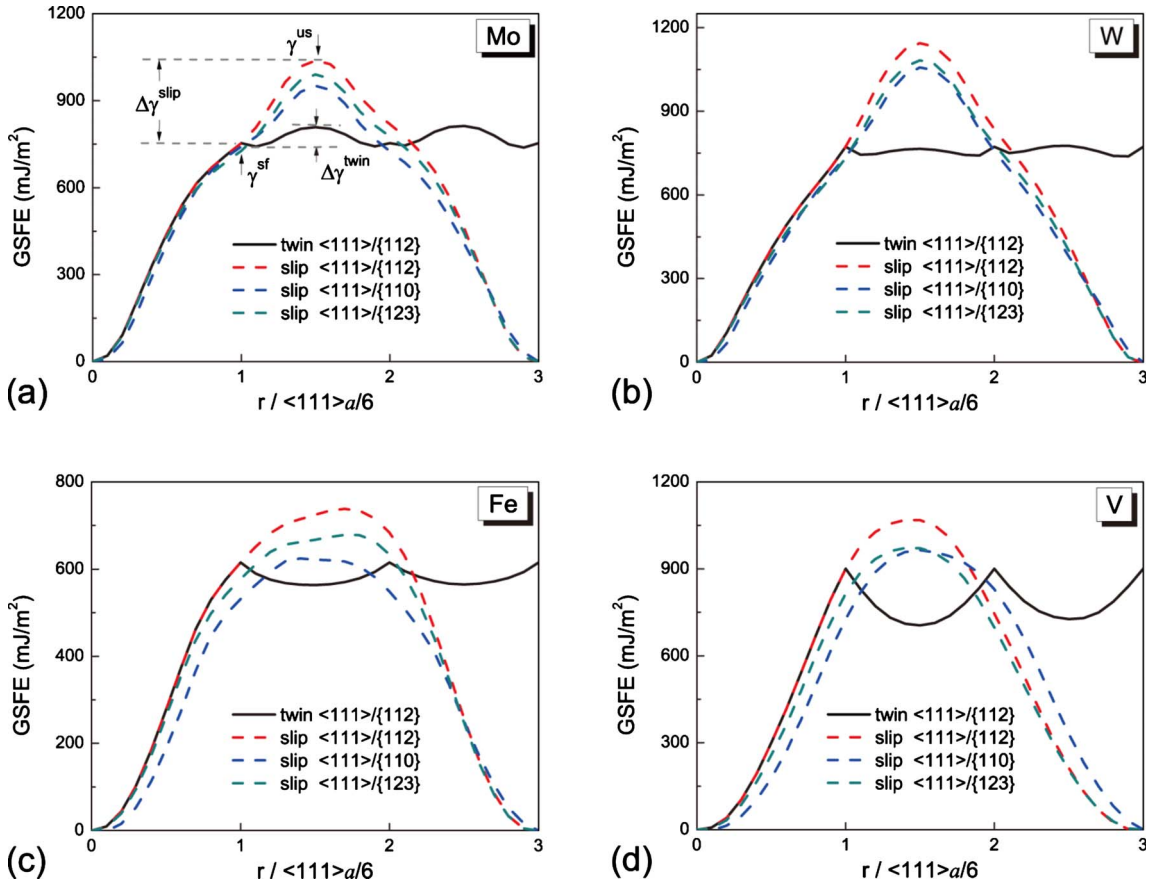

FIG. 10. (Color online) GSFE of BCC Mo, W, Fe, and V crystals, respectively, shown in (a)–(d). The solid and dashed lines represent twinning and full-dislocation slip, respectively. γ^{sf} refers to the barrier for producing stacking fault energy by emission of the first $\frac{a}{6}[111]$ partial. γ^{us} represents the unstable stacking fault energy to induce the full-dislocation slip, which is specifically defined as γ^{us110}, γ^{us112}, and γ^{us123} in the three $\langle 111\rangle/\{110\}$, $\langle 111\rangle/\{112\}$, and $\langle 111\rangle/\{123\}$ systems, respectively. $\Delta\gamma^{twin}$ and $\Delta\gamma^{slip}$ refer to the maximum energy barrier by emission of the subsequent partials for twin growth and full dislocation slip in the presence of pre-existing stacking fault of the $\langle 111\rangle/\{112\}$ system.

methods,[41] i.e., using the periodic boundary conditions along the directions parallel to the shear plane. As shown in Table I, we observe that the difference between γ^{us} in $\langle 111\rangle/\{110\}$, $\langle 111\rangle/\{112\}$, and $\langle 111\rangle/\{123\}$ slip systems and γ^{sf} for nanowires, and in bulk is small in W, Mo, and Fe, but a little larger in V. This results in the changes in $\gamma^{sf}/\min\{\gamma^{us}\}$ and $\Delta\gamma^{twin}/\Delta\gamma^{slip}$ in W, Mo, Fe, and V nanowires. This is reasonable as the surface energies play a crucial role at the nanoscale.[5–9,42]

As the present paper focuses on the deformation behavior at nanoscale, we use the data obtained from the nanowires to analyze the competition between full-dislocation slip and twinning. As shown in Table I, the values of $\gamma^{sf}/\min\{\gamma^{us}\}$ in Mo, W, Fe, and V nanowires are all smaller than 1 (0.73, 0.79, 0.98, and 0.93, respectively). This indicates that in bcc nanowires a $\frac{a}{6}[111]$ partial dislocation is preferred over the $\langle 111\rangle/\{110\}$ and $\langle 111\rangle/\{123\}$ full dislocation slip at the initial stage of deformation.

After the SF induced by one $\frac{a}{6}[111]/(\bar{2}11)$ partial dislocation is formed, it is not clear whether $\langle 111\rangle/\{112\}$ twin or full dislocation will occur from the perfect crystal. It depends on the competition between the energy barrier to emit a $\frac{a}{3}[111]$ trailing dislocation ($\Delta\gamma^{slip}$) to form a full dislocation and the energy to emit a subsequent $\frac{a}{6}[111]$ partial dislocation ($\Delta\gamma^{twin}$) to form a twin. Clearly, the ratio of $\Delta\gamma^{twin}/\Delta\gamma^{slip}$ reflects a competition between twinning and full-dislocation slip, if $\Delta\gamma^{twin}/\Delta\gamma^{slip}>1$, it means the emission of a $\frac{a}{3}[111]$ trailing dislocation on the pre-existing SF is easier, and thus $\langle 111\rangle/\{112\}$ full dislocation is preferred; whereas if $\Delta\gamma^{twin}/\Delta\gamma^{slip}<1$, the emission of a subsequent $\frac{a}{6}[111]$ partial dislocation on the pre-existing SF is easier, and then the $\langle 111\rangle/\{112\}$ twin is preferred.

As shown in Table I, the values of $\Delta\gamma^{twin}/\Delta\gamma^{slip}$ for Mo, W, and Fe nanowires are all smaller than 1 (0.06, 0.23, and 0.42, respectively). This implies that the $\langle 111\rangle/\{112\}$ twin is preferred in Mo, W, and Fe nanowires. However, the value of $\Delta\gamma^{twin}/\Delta\gamma^{slip}$ in V nanowires is larger than 1 (1.15), which indicates that the $\frac{a}{6}[111]/(\bar{2}11)$ full dislocation is preferred in V nanowires. This analysis is also consistent with the atomic configurations in Figs. 5(a)–5(d).

Based on the above understanding, we can further predict the preference for twinning in bcc crystals. As twinning is related to the formation of the SF by a $\frac{a}{6}[111]/(\bar{2}11)$ partial dislocation and then subsequent formation of $\frac{a}{6}[111]$ partials on adjacent $(\bar{2}11)$ planes, it is natural to conclude that due to a smaller value of $\gamma^{sf}/\min\{\gamma^{us}\}$ and $\Delta\gamma^{twin}/\Delta\gamma^{slip}$, it is easier

TABLE I. Calculated γ^{us} for different slip systems, γ^{sf}, $\Delta\gamma^{twin}$, $\Delta\gamma^{slip}$, and $\gamma^{sf}/\min\{\gamma^{us}\}$ in bulk and in nanowires (with size $50a\times5\sqrt{2}a\times5\sqrt{2}a$, where a is the lattice constant at 0 K) of W, Mo, Fe, and V. The energy unit is mJ/m^2.

	W		Mo		Fe		V	
	Nano	Bulk	Nano	Bulk	Nano	Bulk	Nano	Bulk
γ^{us110}	1057	1021	952	902	625	660	965	1075
γ^{us112}	1144	1185	1038	1063	738	766	1069	1238
γ^{us123}	1083	1111	990	1043	679	754	973	1243
γ^{sf}	773	830	754	796	615	649	900	960
$\Delta\gamma^{twin}$	21	61	66	96	52	63	195	198
$\Delta\gamma^{slip}$	371	355	284	266	123	117	169	278
$\gamma^{sf}/\min(\gamma^{us})$	0.73	0.81	0.79	0.88	0.98	0.98	0.93	0.89
$\Delta\gamma^{twin}/\Delta\gamma^{slip}$	0.06	0.17	0.23	0.36	0.42	0.54	1.15	0.71

for the system to form a $\langle111\rangle/\{112\}$ twin. As shown in Table I, both the ratio of $\gamma^{sf}/\min\{\gamma^{us}\}$ and $\Delta\gamma^{twin}/\Delta\gamma^{slip}$ indicate the sequence $W<Mo<Fe<1$. Thus, compared to full dislocation slip systems, the preference for twinning in the present work is given by $W>Mo>Fe$.

D. Comparison of superelasticity between fcc and bcc nanowires

We have demonstrated above that, driven by surface energy minimization, bcc nanowires can show superelasticity through twinning deformation. Combined with the work for fcc systems,[10–12] our present study shows that SE should be a general phenomenon in cubic metal nanowires under the condition of high surface energy and twinning deformation. The minimization of surface energy provides an intrinsic driving force for the transformation between two configurations, and twinning deformation provides the dynamic pathway for the completion of crystal reorientation. However, it is interesting to examine the differences between bcc and fcc nanowires in their superelastic behavior. Here in points (1)–(3) below, we show that although bcc nanowires have similar shape recovery behavior, they behave differently from their fcc counterparts regarding twin formation, twin mobility, energy dissipation, and applications over a wider temperature range.

(1) The GSFE for twinning in bcc metals is obviously different from that of fcc metals, indicating a dramatic difference in twinning formation and mobility between bcc and fcc metals. First, the energy barrier for emitting the first partial to form a SF in a bcc metal is quite large compared to that in a fcc metal. For example, the barrier is 773 mJ/m^2 and 180 mJ/m^2 in W and Cu,[14] respectively. Since the formation of SF is of great importance for nucleation of twins, bcc metals need a large driving force for twinning nucleation compared to fcc metals. Second, the energy barrier for the emission of subsequent partial dislocations for twinning in bcc metals is smaller than that for a full dislocation. In contrast, the energy barrier for the emission of subsequent partial dislocations for twining in fcc metals is larger than that for a full dislocation.[34] Therefore, in bcc metals there is a bigger opportunity for the emission of subsequent partial dislocations, making the formation of twins much easier than that in fcc metals. Then the shape of GSFE curves after SF formation in bcc metals is also significantly different from that of fcc metals. The energy landscape for fcc twinning is always very rugged; in contrast to the flat energy landscape in bcc metals. Thus, bcc metals have a very low twin boundary migration energy and twin boundary motion in bcc metals is easier than in fcc metals [e.g., 21 mJ/m^2 in W vs 157 mJ/m^2 in Cu (Ref. 14)].

(2) The difference in twinning mobility results in obvious differences in stress-strain curves between bcc and fcc metals. In contrast to the typical strain hardening behavior in fcc nanowires, there is no obvious strain hardening in the present study of bcc systems. Most interestingly, the stress-strain curves of the bcc nanowires show quite a small hysteresis and lower energy dissipation during the loading/unloading process that is significantly different from that in fcc crystals. This difference is easily understood in terms of the difference of twin boundary motion barrier between bcc and fcc metals. Due to the very low twin boundary barrier, the twins in bcc nanowires move easily and revert back than their fcc counterparts, leading to the small strain hardening rate and small hysteresis.

(3) Some refractory bcc nanowires, such as W and Mo, can show SE in quite a wide temperature range than that in fcc nanowires. fcc nanowires, e.g., Cu, can only show superealsticity at temperatures lower than 900 K due to the low melting point.[11] Above this temperature, surface diffusion becomes intense, and destroys the nanostructures. However, as bcc W and Mo crystals have extremely high melting points (3695 K and 2896 K, respectively), surface diffusion is not that important at relatively high temperature for these refractory metals. We find that W nanowires can show SE even at temperatures higher than 1500 K (shown in Fig. 11), which exceeds the value for almost all the reported high-temperature shape memory alloys in bulk.[16,17] Such behavior may help the development of high-temperature shape-memory materials at the nanoscale.

Finally, it should be noted that, our further work[43,44] will show that, some hexagonal closed packed structures, e.g., Zr metal nanowires, can also show superelasticity driven by the

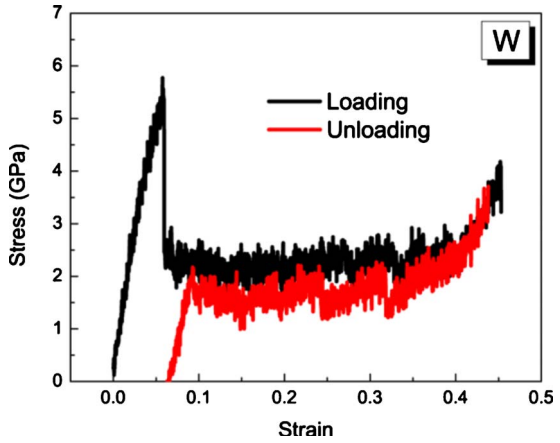

FIG. 11. (Color online) Superelasticity in a W nanowire of dimensions $50a \times 5\sqrt{2}a \times 5\sqrt{2}a$ at high temperature (1500 K), where a is the lattice constant at 0 K.

reduction of surface energy but mediated by an inverse martensitic transformation. This is a pathway for surface energy minimization that completely differs from that in fcc and bcc metal nanowires. Combined with the present work on bcc nanowires and previous studies on fcc nanowires, it clearly shows that superelasticity should be even more general in metal nanowires and the driving force comes from the same origin—the reduction in surface energy of the nanowire.

V. CONCLUSION

We have used molecular-dynamics simulations to study the mechanical behavior of bcc single-crystalline nanowires. Our main conclusions can be summarized as follows: (1) driven by surface energy minimization, bcc nanowires (Mo, W, and Fe) can show superelasticity through twin deformation. The superelasticity in bcc nanowires, in association with the observed superealsticity in fcc nanowires,[10–12] suggests that superelasticity is a general phenomenon in cubic metal nanowires under the conditions of high surface energy and twinning deformation. The minimization of surface energy provides an intrinsic driving force for the transformation between two configurations and twinning deformation provides the dynamical path for the complete crystal reorientation. (2) In bcc nanowires, the $\langle 111\rangle/\{112\}$ stacking fault generated by $\frac{a}{6}\langle 111\rangle$ partial dislocations is always preferred over the $\langle 111\rangle/\{110\}$ and $\langle 111\rangle/\{123\}$ full dislocation slip. However, whether a $\langle 111\rangle/\{112\}$ twin or a $\langle 111\rangle/\{112\}$ full dislocation slip is preferred in bcc nanowires depends on the competition between the emission of a subsequent $\frac{a}{6}\langle 111\rangle$ partial dislocation on adjacent $\{112\}$ planes and the emission of a $\frac{a}{3}\langle 111\rangle$ partial in the same plane. If the energy barrier for emission of consecutive $\frac{a}{6}\langle 111\rangle$ partials adjacent to the pre-existing stacking fault is lower than that for a $\frac{a}{3}\langle 111\rangle$ partial on the pre-existing SF, a $\langle 111\rangle/\{112\}$ twin is preferred. (3) The generalized stacking fault energy for twinning in bcc metals is quite different than that of fcc metals. Thus, the bcc metal has a higher energy barrier for the nucleation of a twin, but a lower energy barrier for twin formation and migration, which results in some unique characteristics of the superelasticity in bcc nanowires, such as low-energy dissipation and low strain hardening. (4) Due to their extremely high melting points, refractory Mo and W nanowires can show superelasticity at very high temperatures, exceeding the temperature for fcc shape-memory nanowires and almost all the reported high-temperature shape memory alloys in bulk.

ACKNOWLEDGMENTS

This work was supported by NSFC (Grants No. 50771079, No. 50720145101, and No. 50831004) and the 973 Program of China (Grant No. 2010CB631003) as well as 111 project (B06025) of China. X.D., T.L. and A.S. also acknowledge support from the U.S. DOE at LANL (Grant No. DE-AC52-06NA25396). J.L. acknowledges support by NSF under Grant No. CMMI-0728069, MRSEC under Grant No. DMR-0520020, ONR under Grant No. N00014-05-1-0504, and AFOSR under Grant No. FA9550-08-1-0325.

*Corresponding author.
†dingxd@mail.xjtu.edu.cn
‡txl@lanl.gov

[1] K. Otsuka and X. Ren, Prog. Mater. Sci. **50**, 511 (2005).
[2] K. Otsuka and T. Kakeshita, MRS Bull. **27**, 91 (2002).
[3] A. Planes and L. Manosa, Solid State Phys. **55**, 159 (2001).
[4] X. Ding, T. Suzuki, X. Ren, J. Sun, and K. Otsuka, Phys. Rev. B **74**, 104111 (2006).
[5] A. Saxena and G. Aeppli, MRS Bull. **34**, 804 (2009).
[6] R. Dingreville, J. M. Qu, and M. Cherkaoui, J. Mech. Phys. Solids **53**, 1827 (2005).
[7] S. Auer and D. Frenkel, Nature (London) **413**, 711 (2001).
[8] T. Lookman and P. Littlewood, MRS Bull. **34**, 822 (2009).
[9] T. Waitz, K. Tsuchiya, T. Antretter, and F. D. Fischer, MRS Bull. **34**, 814 (2009).
[10] J. Diao, K. Gall, and M. L. Dunn, Phys. Rev. B **70**, 075413 (2004).
[11] W. Liang, M. Zhou, and F. Ke, Nano Lett. **5**, 2039 (2005).
[12] H. S. Park, K. Gall, and J. A. Zimmerman, Phys. Rev. Lett. **95**, 255504 (2005).
[13] H. S. Park and C. J. Ji, Acta Mater. **54**, 2645 (2006).
[14] W. Liang and M. Zhou, Phys. Rev. B **73**, 115409 (2006).
[15] W. Liang and M. Zhou, ASME J. Eng. Mater. Technol. **127**, 423 (2005).
[16] P. J. S. Buenconsejo, H. Y. Kim, H. Hosoda, and S. Miyazaki, Acta Mater. **57**, 1068 (2009).
[17] K. Chastaing, A. Denquin, R. Portier, and P. Vermaut, Mater. Sci. Eng., A **481-482**, 702 (2008).
[18] M. I. Mendelev, S. Han, D. J. Srolovitz, G. J. Ackland, D. Y. Sun, and M. Asta, Philos. Mag. **83**, 3977 (2003).
[19] M. I. Mendelev, S. Han, W. J. Son, G. J. Ackland, and D. J. Srolovitz, Phys. Rev. B **76**, 214105 (2007).

[20] M. W. Finnis and J. E. Sinclair, Philos. Mag. A **50**, 45 (1984).
[21] M. S. Daw and M. I. Baskes, Phys. Rev. B **29**, 6443 (1984).
[22] S. Nosé, J. Chem. Phys. **81**, 511 (1984).
[23] W. G. Hoover, Phys. Rev. A **31**, 1695 (1985).
[24] S. Plimpton, J. Comput. Phys. **117**, 1 (1995).
[25] J. Li, Modell. Simul. Mater. Sci. Eng. **11**, 173 (2003).
[26] A. Machová and G. J. Ackland, Modell. Simul. Mater. Sci. Eng. **6**, 521 (1998).
[27] V. Shastry and D. Farkas, Modell. Simul. Mater. Sci. Eng. **4**, 473 (1996).
[28] Z. Y. Huo, C. K. Tsung, W. Y. Huang, X. F. Zhang, and P. D. Yang, Nano Lett. **8**, 2041 (2008).
[29] Y. Kondo and K. Takayanagi, Phys. Rev. Lett. **79**, 3455 (1997).
[30] J. W. Christian and S. Mahajan, Prog. Mater. Sci. **39**, 1 (1995).
[31] B. Q. Li, M. L. Sui, B. Li, E. Ma, and S. X. Mao, Phys. Rev. Lett. **102**, 205504 (2009).
[32] J. K. Diao, K. Gall, and M. L. Dunn, Nature Mater. **2**, 656 (2003).
[33] J. R. Rice, J. Mech. Phys. Solids **40**, 239 (1992).
[34] E. B. Tadmor and S. Hai, J. Mech. Phys. Solids **51**, 765 (2003).
[35] H. Van Swygenhoven, P. M. Derlet, and A. G. Froseth, Nature Mater. **3**, 399 (2004).
[36] S. Kibey, J. B. Liu, D. D. Johnson, and H. Sehitoglu, Acta Mater. **55**, 6843 (2007).
[37] J. W. Christian, Metall. Trans. A **14**, 1237 (1983).
[38] K. Ito and V. Vitek, Philos. Mag. A **81**, 1387 (2001).
[39] V. Vítek, Philos. Mag. **18**, 773 (1968).
[40] S. Ogata, J. Li, and S. Yip, Phys. Rev. B **71**, 224102 (2005).
[41] J. A. Zimmerman, H. J. Gao, and F. F. Abraham, Modell. Simul. Mater. Sci. Eng. **8**, 103 (2000).
[42] Y. M. Juan, Y. M. Sun, and E. Kaxiras, Philos. Mag. Lett. **73**, 233 (1996).
[43] S. Li, X. Ding, J. Li, X. Ren, J. Sun, E. Ma, and T. Lookman, Phys. Rev. B **81**, 245433 (2010).
[44] S. Li, X. Ding, X. Ren, J. Sun, T. Lookman, and A. Saxena (unpublished).